Pattern formation during the oscillatory photoelectrodissolution of n-type silicon: Turbulence, clusters and chimeras

Konrad Schönleber, Carla Zensen, Andreas Heinrich and Katharina Krischer

March 20, 2014

arXiv:1403.4825v1 [nlin.PS] 19 Mar 2014

We report and classify the rich variety of patterns forming spontaneously in the oxide layer during the oscillatory photoelectrodissolution of n-type doped silicon electrodes under limited illumination. Remarkably, these patterns are often comprised of several dynamical states coexisting on the electrode, such as subharmonic phase clusters and spatio-temporal chaos, and include so-called 'chimera states'. The experiments suggest that the subharmonic phase clusters emerge from a period doubling bifurcation which, upon further parameter changes, evolve into classical phase clusters. Experimentally the occurrence of the patterns is controlled via two coupling mechanisms: A linear global coupling by an external resistor and a nonlinear coupling imposed on the system by the limitation of the illumination.

1 Introduction

Oscillatory media are known to exhibit a variety of spatial patterns [1, 2]. Best known are spiral waves and chemical turbulence, as most famously encountered in the Belousov-Zhabotinsky (BZ) reaction or the oxidation of CO on Pt in UHV [3, 4, 5, 6]. These systems can be understood as ensembles of diffusively coupled individual oscillators. Additionally, there are many physical mechanisms leading to a long range or even global coupling of the oscillators. This applies, e.g., to electrically controlled systems, such as semiconductor devices [7, 8], gas discharge tubes [9] or electrochemical systems [10, 11, 12, 13]. The most prominent patterns emerging from a global coupling are scale free cluster patterns where the medium separates into a few domains, oscillating with a certain, constant phase lag [14, 15, 16, 17, 18]. Properties of these cluster patterns have been intensely studied theoretically employing phase oscillator models or the complex Ginzburg-Landau equation with linear global coupling [19, 20]. Yet, the exploration of the phenomena occurring and the understanding of the dynamics of these patterns is far from being complete. In this article, we present a collection of peculiar patterns and unusual synchronization phenomena observed in an electrochemical experiment, the oscillatory photoelectrodissolution of n-type silicon, and their classification.

During the electrodissolution the silicon is first oxidized electrochemically according to the following reaction [21]:

$$\mathrm{Si} + 2\mathrm{H_2O} + \nu_{\mathrm{VB}} h^+ \rightarrow \mathrm{SiO_2} + 4\mathrm{H^+} + (4 - \nu_{\mathrm{VB}}) e^- \qquad (1)$$

where ν_{VB} denotes the number of charge transfer processes via the valence band of the silicon, i.e., processes involving minority charge carriers in n-type silicon. This oxide is subsequently etched away by fluoride species present in the electrolyte in a purely chemical process. For n-type doped silicon, the dominant spatial coupling mechanism between the oscillators involves the diffusion of holes. The holes drive the initial charge transfer step in equation 1, i.e., the inequality $\nu_{\mathrm{VB}} \geq 1$ holds [22]. A limited illumination and, therefore, limited generation rate of holes in the valence band of the working electrode thus introduces a cut-off for the total current. Clearly, this mechanism has a nonlinear coupling characteristic. An additional global coupling mechanism is introduced by connecting a resistance R_{ext} in series to the working electrode in the potentiostatically controlled experiments. This external resistance thus couples the voltage drop $\Delta\phi_{\mathrm{int}}$ across the electrode|oxide|electrolyte interface at each individual point of the surface of the working electrode to the total current through the working electrode and consequently has a linear characteristic.

$$\Delta\phi_{\mathrm{int}} = U - R_{\mathrm{ext}} A \cdot \bar{j} \qquad (2)$$

Here, U is the externally applied voltage, $\bar{j}$ the spatial average of the current density and A the electrode area.

In order to get a comprehensive picture of the dependence of the patterns on the experimental parameters, four of these parameters are varied over a wide range where current oscillations occur. Two of these parameters characterize the electrolyte, the first one being the total concentration of fluoride species c_{F} and the second one the pH value which determines the distribution of the fluoride on the three species $\mathrm{F^-}$, HF and $\mathrm{HF_2^-}$ according to the law of mass action. Both parameters together determine the total silicon oxide etching rate as the different fluoride species follow different etching pathways with distinct rates [23, 24]. The other two parameters represent the strengths of the coupling mechanisms given by the illumination intensity I_{ill} for the nonlinear coupling and $R_{\mathrm{ext}}A$ for the purely linear global coupling, respectively.

2 Experimental

The working electrodes are the (111) faces of monocrystalline, n-type doped silicon samples with a resistivity of $3 - 5\ \Omega$cm. They are ohmically back-contacted with a thermally evaporated 200 nm aluminum layer annealed at 250 °C for 15 minutes. The silicon is attached to a custom made PTFE holder via silicone paste (Scrintex 901, Ralicks GmbH, Rees-Haldern, Germany) which also serves as a sealing for the back-contact against the electrolyte. The typical electrode size is $A \approx 4 \times 6$ mm^2. As a counter electrode, a circular shaped platinum wire is placed symmetrically in front of the working electrode and a $\mathrm{Hg|Hg_2SO_4}$ reference electrode is used which is placed behind the working electrode at a distance of several centimeters. During the experiments the electrolyte is constantly stirred with a magnetic stirrer rotating at about 10 Hz. The sample illumination is realized by a He-Ne laser and the illumination intensity is adjusted by a polarizer plate.

The laser beam is optically expanded to a diameter of ca. 1.5 cm and passes an iris diaphragm so that only its central part is incident on the sample to guarantee a spatially uniform illumination.

For the ellipsometric imaging of the optical path through the oxide, light from a blue LED (λ = 470 nm) is first elliptically polarized by passing a linear polarizer and a zeroth order $\lambda/4$-plate. It then hits the sample surface at an angle close to the Brewster angle of the silicon|electrolyte system ($\approx 70°$). The reflected light passes another polarizer which converts changes in the polarization upon reflection caused by the optical path through the oxide into an intensity signal. Using a suitable lens, an image of this ellipsometric intensity distribution across the surface is then created on the CCD chip of a camera (JAI CV-A50). The data is then digitized using a frame grabber card (PCI-1405, National Instruments) and preprocessed and recorded by a Labview program. A sketch of the setup (with the optical components of the ellipsometric imaging path omitted) is shown in figure 1.

Before the experiments the silicon working electrodes

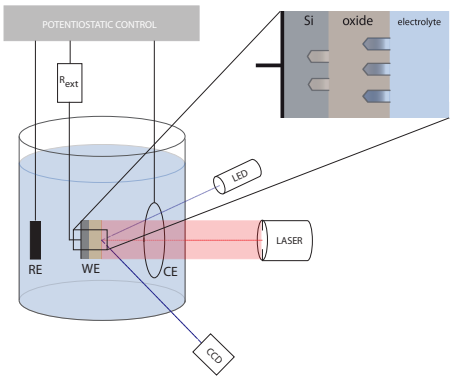

Figure 1: Sketch of the experimental setup showing the arrangement of the three electrodes and the external resistance together with the optical paths for the sample illumination (red) and the spatially resolved ellipsometric imaging (blue). A cross section of the interface and the growth direction of the oxide is shown in the inset. A schematic of the optical components in the light path between the LED and the CCD can be found in [25]

are cleaned by first rubbing them carefully with an acetone soaked tissue and subsequently immersing them acetone (p.a.), ethanol (p.a.), methanol (p.a.) and ultrapure water for 5 min each. The electrolyte is always an aqueous solution of NH_4F (Merck, p.a.) as a fluoride source and H_2SO_4 (Merck, Suprapur) to adjust the pH value. Prior to the experiments the electrolyte is bubbled with argon and an argon atmosphere is retained during the experiments.

All experiments are potentiostatically controlled (FHI-2740, electronics laboratory of the Fritz-Haber- Institut, Berlin, Germany). A constant voltage of 8.65 V vs. SHE is applied between the reference and the working electrode with a tunable ohmic resistance connected in series to the working electrode.

For the analysis of the patterns the spatial distribution of the ellipsometric intensity at specified points in time is considered as well as the ellipsometric signal of one dimensional subsets of the electrode over the entire time window. Furthermore, the time series of the ellipsometric intensity at each individual point is Fourier transformed (FFT, MATLAB) and the spatial distribution of absolute value and phase of relevant Fourier coefficients is then used to gain insight into phase clustering behavior for these Fourier modes. Lastly, the data from a selected area on the electrode is Hilbert transformed (MATLAB) and the resulting analytical signal is used to visualize the different dynamics on the electrode.

3 Results and Discussion

3.1 Overview

Parameter variation

The occurrence of oscillations and the accompanying pattern formation for a given electrolyte depends on the respective strengths of the two coupling mechanisms, i.e., on the values of the external resistance $R_{\mathrm{ext}}A$ and the illumination intensity I_{ill}. An examplary 2d parameter space is shown in figure 2. If

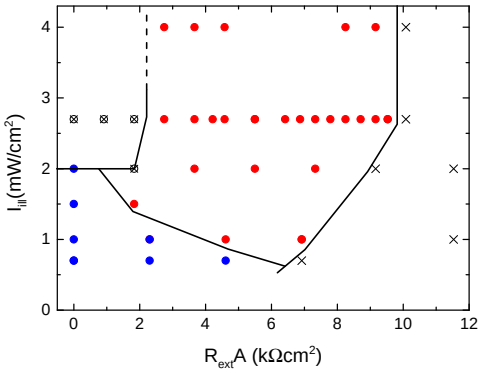

Figure 2: Dependence of the oscillatory and pattern forming regime on the external resistance $R_{\mathrm{ext}}A$ and the illumination intensity I_{ill} for an electrolyte with c_{F}=50 mM and pH 2.3. Uniform oscillations (red) and oscillations accompanied by spatial pattern formation (blue) are shown together with stable fixed points with (circle) and without (cross) an oscillatory transient outside of the oscillatory regime. The borders of the oscillatory and the pattern forming regime are indicated by lines.

the total coupling is too weak, i.e., at high I_{ill} and low R_{ext}, the system settles to a stable focus. Conversely, if the total coupling becomes too strong, the system relaxes monotonically to a stable node. If the nonlinear coupling is weak, i.e., for relatively high illumination intensities, the entire electrode oscillates uniformly reflecting a strong synchronizing spatial coupling. An example for such a uniform oscillation is shown in figure 3.

Uniform oscillations are also found in all oscillatory measurements at non-illuminated p-type silicon samples as discussed in detailed studies of such samples conducted previously in our group [25, 26]. In addition to the uniformity, the shape of the oscillations for highly illuminated n-type doped silicon and p-type doped silicon samples are identical at otherwise matched experimental parameters and in both cases a minimal external resistance has to be introduced. This similarity in behavior can be fully attributed to the sufficiencyof the

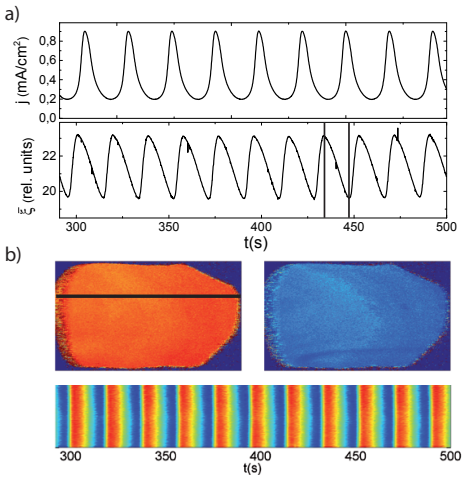

Figure 3: Uniform oscillation of the electrode at a high illumination intensity ($c_F = 75$ mM, pH = 1, $R_{ext}A = 6.51$ kΩcm^2, $I_{ill} = 5.85$ mW/cm^2). **a)** Time series of the global quantities j and $\overline{\xi}$; **b)** Ellipsometric intensity distribution on the electrode for the two times indicated by the vertical lines in a) and the temporal evolution of a 1d cut along the line indicated in the left electrode picture. Red indicates a relatively high and blue a relatively low ellipsometric intensity.

amount of holes in the valence band to maintain the current present in both cases, strongly corroborating the notion that the nonlinear coupling introduced by the restriction of holes is solely responsible for the emergence of patterns. Consequently, in the parameter space shown in figure 2 only at illumination intensities below an electrolyte specific threshold value of $I_{ill} = 2.5$ mW/cm^2 pattern formation can be observed. If the linear global coupling is chosen too strong, the patterns vanish and uniform oscillations are observed although the current is still restricted by the illumination and an effect of the nonlinear coupling is thus still to be expected. This behavior is in accordance with literature where the global coupling through an external resistor tends to synchronize the oscillations, at least when the electrode potential acts as the activator [27, 28]. As a consequence patterns are only found in the parameter region where the nonlinear coupling dominates the linear global coupling, i.e., in the lower left hand corner of figure 2. Most notably, here, sustained oscillations are observed even without an external resistance.

Pattern classification

Compared to patterns classically found in oscillatory media the silicon oscillator exhibits two characteristic and peculiar phenomena: First, in a large part of the pattern forming parameter region the global quantities, i.e., the total current j and the spatially averaged ellipsometric intensity $\overline{\xi}$ oscillate in a simple periodic fashion although local time series exhibit complex oscillation forms up to completely irregular ones. Besides, $\overline{\xi}$ may oscillate with a period-2 or irregularly. Second, typically different dynamic behaviors as for example cluster patterns and spatio-temporal chaos coexist on the electrode. We call a part of the surface with one distinct dynamics a region.

In the following we classify the patterns, in a first step, according to the spatially averaged ellipsometric intensity $\overline{\xi}$ into three categories:

- Simple periodic oscillations
- Period-2 oscillations
- Oscillations with an irregular amplitude

Exemplary time series for the three types of $\overline{\xi}$ oscillations are shown in figure 4. In the case of simple periodic oscillations

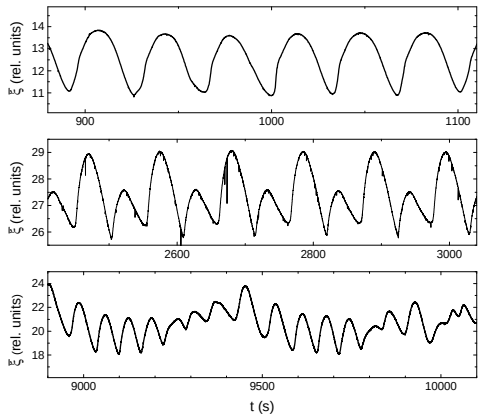

Figure 4: Time series of the spatially averaged ellipsometric intensity $\overline{\xi}$ for three different measurements showing simple periodic oscillations (top), period-2 oscillations (middle) and oscillations with an irregular amplitude (bottom).

in $\overline{\xi}$, 2d simulations using the suitably modified complex Ginzburg-Landau equation with a nonlinear global coupling show striking similarities with the patterns observed in the experiments [29, 30, 31]. This opens a pathway to a possible deeper understanding of both the origin of the pattern formation and the coupling mechanism. Consequently, in the following the emphasis is first put on the analysis of the first class of patterns and the second and third class are treated as modifications of this first class and are discussed later.

3.2 Simple periodic oscillations in $\overline{\xi}$

In a first step we now consider the patterns forming during simple periodic $\overline{\xi}$ oscillations depicted in the top of figure 4. The regularity of the spatially averaged signal implies that the spatial variations of the patterns cancel out on average. There are two dominant types of patterns forming. First, subharmonic phase clusters are found, where the ellipsometric intensity at each point shows oscillations with a strong frequency component at an integer fraction of the spatially averaged oscillation frequency. These points are arranged in phase domains where all points within a domain are synchronized and the distinct domains differ in their phase [29]. Typically but not exclusively, 2-phase clusters are found. The second type of dynamical behavior found are desynchronized oscillations with a broad distribution of oscillation frequencies. Hence, at any given point the oscillation amplitude is irregular.

As already mentioned, typically the electrode forms different regions. In a region either one of the two patterns mentioned or a synchronized oscillation with the frequency of the spatially averaged signal exists. The occurrence of only one type of dynamical behavior on the entire electrode surface and any pairwise coexistence have been found in this study and are subsequently presented.

One region

First, we take a look at the patterns with only one region covering the entire electrode. We start by discussing 2-phase clusters. An example is shown in figure 5. As apparent from

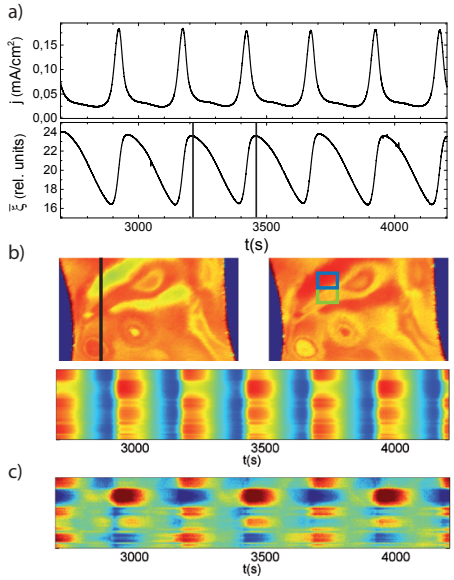

Figure 5: Subharmonic cluster pattern covering the entire electrode (c_F = 35 mM, pH = 1, $R_{ext}A$ = 9.1 kΩcm^2, I_{ill} = 0.7 mW/cm^2). **a)** Time series of j and $\bar{\xi}$; **b)** Ellipsometric intensity distribution on the electrode for the two times indicated by the vertical lines in a) and the temporal evolution of a 1d cut along the line indicated in the left electrode picture. Red indicates a relatively high and blue a relatively low ellipsometric intensity; **c)** 1d cut as in b) where $\bar{\xi}$ is subtracted from every local time series. The color scale is not identical to b).

figure 5 a) the spatially averaged ellipsometric intensity $\bar{\xi}$ as well as the spatially averaged current density j oscillate in a simple periodic fashion. At the same time this oscillation is not uniform as can be seen in figure 5 b) where two snapshots of the ellipsometric images and the temporal evolution of a 1d cross section are depicted. Clearly, at every point, an amplitude variation can be seen which inverts every other oscillation. For a better visibility of the spatial distribution of the amplitude variations the underlying uniform oscillation is subtracted in subfigure 5 c), uncovering subharmonic local oscillations. The characteristics of this structure are further elucidated by the results of a pointwise Fourier analysis in figure 6. In subfigure 6 a), the spatial average of the absolute values of the pointwise Fourier spectra is compared to the Fourier spectrum of the spatially averaged ellipsometric intensity. The occurrence of an additional peak at half the dominant frequency can clearly be seen. The spatial distribution of absolute value and phase of the Fourier coefficient corresponding to this additional, subharmonic frequency are shown in figure 6 b). The latter is composed of two values which are about π apart, confirming that a 2-phase cluster spreading across the entire electrode area is indeed present. The two clustered phase domains are separated by Ising-type walls, i.e., by a zero crossing of the absolute value of the Fourier coefficient where the phase jump occurs. This manifests in the black lines in the left hand picture of figure 6 b).

More insight into the details of the cluster dynamics can

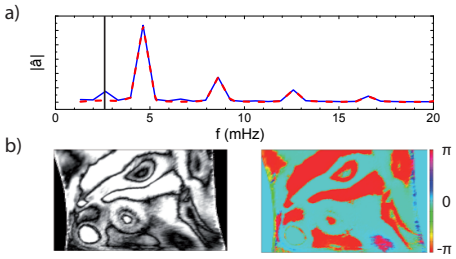

Figure 6: Fourier analysis of the subharmonic cluster pattern shown in figure 5. **a)** Spatial average of the absolute values of the pointwise Fourier spectra (blue) and Fourier spectrum of the spatially averaged signal $\bar{\xi}$ (red); **b)** Spatial distribution of the absolute value (left) and phase (right) of the Fourier coefficient corresponding to the Fourier mode indicated by the vertical line in the Fourier spectra in a).

be gained by considering the analytical signal of points from the individual phase domains as shown in figure 7. The ana-

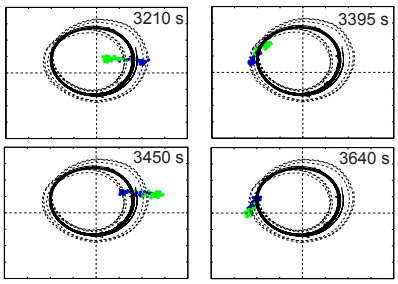

Figure 7: Analytical signal from the points indicated by correspondingly color coded rectangles in figure 5 b) at four consecutive extrema of the $\bar{\xi}$ oscillation shown in figure 5 a) together with the traces of the analytical signal of $\bar{\xi}$ (solid) and a point located in the center of the blue rectangle in figure 5 (dash).

lytical signal of the points in the two areas indicated in figure 5 are arranged on a bar (blue and green points, respectively) whose center follows the analytical signal of $\bar{\xi}$ (black solid line). The end points of the bar, i.e., the points from the individual phase domains, trace a Moebius strip projected on the complex plane. This suggests that the subharmonic clusters result from a period doubling bifurcation of the uniform oscillation. The four snapshots in figure 7 are taken at consecutive extrema of $\bar{\xi}$ and the sequence of pictures thus shows that a full rotation of the bar is accompanied by two full rotations of its center.

The second type of dynamical pattern covering the entire active area observed is a desynchronized oscillation spreading across the entire electrode as shown in figure 8. Here, the remarkable case is shown where the ensemble of pointwise time series of the ellipsometric intensity across the surface is oscillating in a desynchronized manner, while in the spatially averaged signal these differences cancel out almost perfectly leaving a simple periodic oscillation in $\bar{\xi}$ and j. The corresponding full analytical signal of two sets of points on the electrode further illustrates this behavior. It is shown in figure 9. The trajectories of the individual points are uncorrelated, both within the two areas shown and between them, leading to broad point clouds circling the origin.

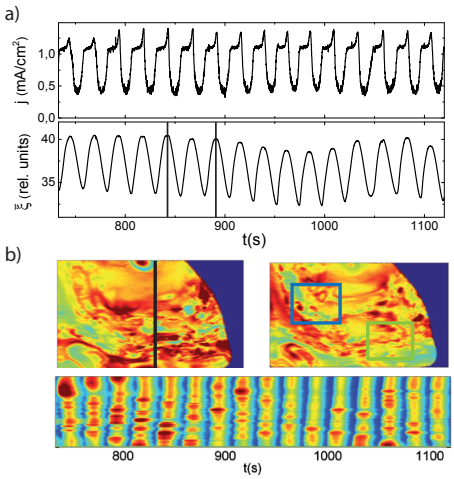

Figure 8: Desynchronized oscillation pattern covering the entire electrode (c_F = 75 mM, pH = 1, $R_{ext}A$ = 0 kΩcm^2, I_{ill} = 2.0 mW/cm^2). **a)** Time series of j and $\bar{\xi}$; **b)** Ellipsometric intensity distribution on the electrode for the two times indicated by the vertical lines in a) and the temporal evolution of a 1d cut along the line indicated in the left electrode picture. Red indicates a relatively high and blue a relatively low ellipsometric intensity.

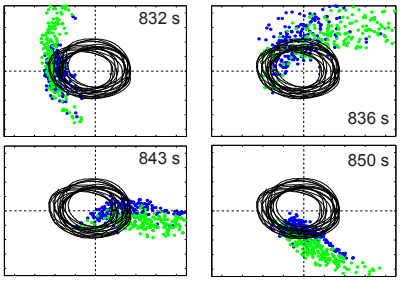

Figure 9: Analytical signal from the points indicated by correspondingly color coded rectangles in figure 8 b) at four points during one oscillation period of the $\bar{\xi}$ oscillation shown in figure 8 a) together with the trace of the analytical signal of $\bar{\xi}$ (solid).

Two regions

A region of one distinct dynamical behavior is typically not covering the entire electrode. More often two such regions are observed to coexist on the electrode. In figure 10 an example for the coexistence of a 2-phase cluster with an approximately synchronous oscillation with the frequency of the spatially averaged signal is depicted. The two regions are clearly distinguishable in figure 10 b) with the 2-phase cluster showing a remarkably fine structured border between its two phase domains. Note that the spatially averaged signals still oscillate in a simple periodic manner.

The Fourier analysis of this pattern is shown in figure 11. Outside the clustered domain the subharmonic frequency is inactive as can be seen in figure 11 b). As in the experiment where the 2-phase cluster covers the entire electrode shown in figures 5-7, the domain walls are Ising-type walls. The analytical signal of points from three areas on the electrode is shown in figure 12. Two main results can be read from the analytical signal in figure 12. First, the center of the rotating bar formed by the two domains of the 2-phase cluster and their

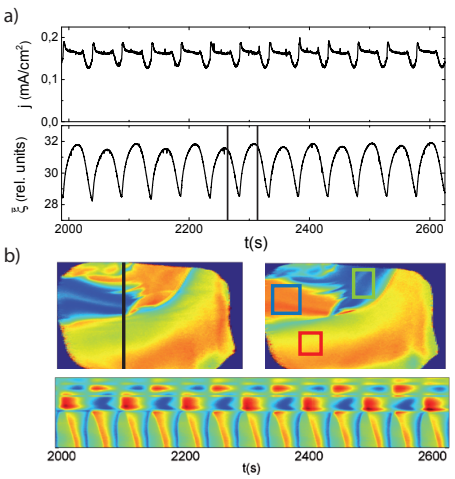

Figure 10: Analysis of a pattern consisting of a synchronized region coexisting with a subharmonic 2-phase cluster (c_F = 50 mM, pH = 1, $R_{ext}A$ = 0.69 kΩcm^2, I_{ill} = 0.4 mW/cm^2). **a)** Time series of j and $\bar{\xi}$; **b)** Ellipsometric intensity distribution on the electrode for the two times indicated by the vertical lines in a) and the temporal evolution of a 1d cut along the line indicated in the left electrode picture. Red indicates a relatively high and blue a relatively low ellipsometric intensity.

separating wall is now approximately stationary in the origin. This means that the underlying harmonic frequency of the spatially averaged signal is strongly suppressed in the region of the 2-phase cluster. Second, the trajectory of the points taken from the approximately synchronized region does not follow the trace of the spatially averaged analytical signal perfectly. This can also be seen in the one dimensional cut in figure 10 b) where the active phase seems to propagate across the surface. We treat this, however, as a minor variation of a perfectly uniform oscillating region. Actually, the region oscillating with the frequency of the spatially averaged signal in a synchronous manner tends to this wave-like disturbance easily.

An interesting point arises comparing the measurement where the 2-phase cluster covers the entire electrode shown in figures 5-7 to the measurement showing coexistence of the 2-phase cluster and synchronized, harmonic oscillation shown in figures 10-12. The transition from the former to the latter dynamical state is seemingly achieved by spatially decomposing the two active frequencies. This is best seen by the corresponding deconvolution of the movement of the bar in the analytical signal shown in figure 7 into a pure rotation of the bar around the origin and a pure center of mass rotation around the origin in the different regions on the electrode as shown in figure 12. The frequency ratio between the center of mass movement and the rotation of the bar remains unaffectedly 1:0.5. A further investigation of this possible deconvolution process would be desirable.

The next case frequently found in the experiments is the coexistence of a synchronized and a desynchronized region on the electrode. This dynamical state is typically called 'chimera state' and has attracted a lot of research interest recently [32, 33, 34, 35, 36, 37]. While in most experiments in literature these states have to be initialized in a special way, their spontaneous occurrence in our system is especially interesting [38]. An exemplary 'chimera state' is shown in

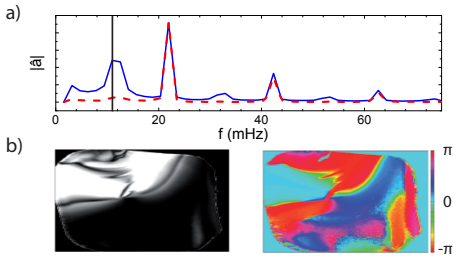

Figure 11: Fourier analysis of the pattern shown in figure 10. **a)** Spatial average of the absolute values of the pointwise Fourier spectra (blue) and Fourier spectrum of the spatially averaged signal $\overline{\xi}$ (red); **b)** Spatial distribution of the absolute value (left) and phase (right) of the Fourier coefficient corresponding to the Fourier mode indicated by the vertical line in the Fourier spectra in a).

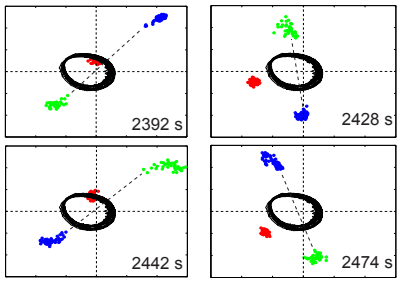

Figure 12: Analytical signal from the points indicated by correspondingly color coded rectangles in figure 10 b) at four points during two oscillation periods of the $\overline{\xi}$ oscillation shown in figure 10 a) together with the trace of the analytical signal of $\overline{\xi}$ (solid). The dashed line represents points in the Ising wall between the two phase domains.

figure 13. Note that while a region of desynchronized local oscillations can easily be seen in figure 13 b), the spatial average is again unaffected. Furthermore, the region of synchronized oscillations seems to be less perturbed by the presence of the region of desynchronized oscillations than by the presence of the subharmonic 2-phase cluster as discussed for figure 10. The coexistence of the two dynamical regions is further emphasized in figure 14 where the analytical signal of points from three areas on the surface shows the qualitative difference between the synchronized and the desynchronized oscillations. Another type of coexistence of synchronized and desynchronized patches on the electrode arises in the case of the coexistence of a 2-phase cluster with a desynchronized region as shown in figure 15. Here, the individual domains in the 2-phase cluster are again synchronized, show a phase difference of π and are separated by Ising-type walls. This is further elucidated in the analytical signal obtained from points spreading across the Ising-type wall in figure 16 (blue and green points). Comparable to figure 7 these points form a bar that rotates at half the angular frequency of the $\overline{\xi}$ oscillation. In contrast, the points from the desynchronized region, displayed in red, spread out in a cloud. As this pattern state is again showing the coexistence of synchronized and desynchronized regions one might argue that it could also be called a 'chimera state'. It has to be noted that a slight period-2 perturbation is visible in the oscillation of $\overline{\xi}$ in figures 15 and 16. This point will be further discussed in section 3.3.

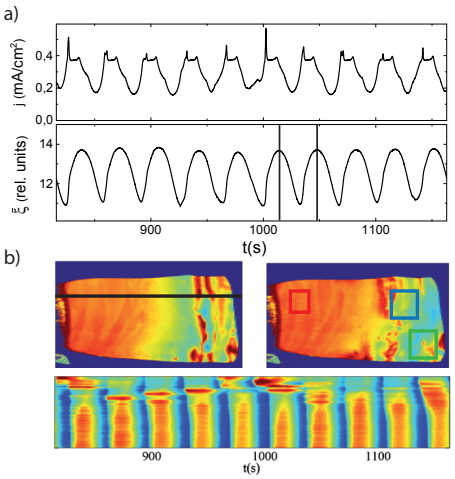

Figure 13: Analysis of a pattern consisting of a synchronized and a desynchronized region (c_F = 75 mM, pH = 3.5, $R_{ext}A$ = 5.61 kΩcm^2, I_{ill} = 1.8 mW/cm^2). **a)** Time series of j and $\overline{\xi}$; **b)** Ellipsometric intensity distribution on the electrode for the two times indicated by the vertical lines in a) and the temporal evolution of a 1d cut along the line indicated in the left electrode picture. Red indicates a relatively high and blue a relatively low ellipsometric intensity.

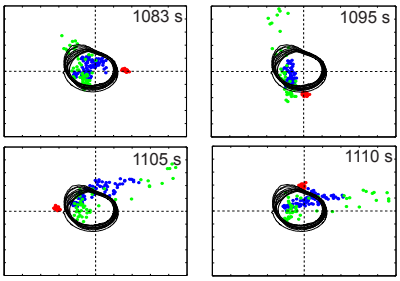

Figure 14: Analytical signal from the points indicated by correspondingly color coded rectangles in figure 13 b) at four points during one oscillation period of the $\overline{\xi}$ oscillation shown in figure 13 a) together with the trace of the analytical signal of $\overline{\xi}$ (solid).

The coexistence of 2-phase clusters with a synchronous simple periodic oscillation as well as chimera states discussed above have also been observed in two other contexts. Tinsley et al. observed them experimentally in a network of coupled chemical oscillators and reproduced the dynamics with a reduced two group model [35]. Here the two groups were obtained by the introduction of a non-local feedback. Furthermore, the uniform oscillation was always stable and thus special initial conditions had to be prepared. This is in contrast to the work described here as well as to the predictions of the modified complex Ginzburg-Landau equation where the patterns occur spontaneously in a purely globally coupled system [31].

3.3 Period-2 oscillations in $\overline{\xi}$

A first deviation from the simple periodic oscillations in $\overline{\xi}$ is the occurrence of period-2 oscillations in $\overline{\xi}$ as shown in the middle of figure 4. In all experiments where this behavior is found it is accompanied by the formation of a 2-phase cluster region where one phase domain covers a larger area or has a higher amplitude in the subharmonic mode than the other. An example is

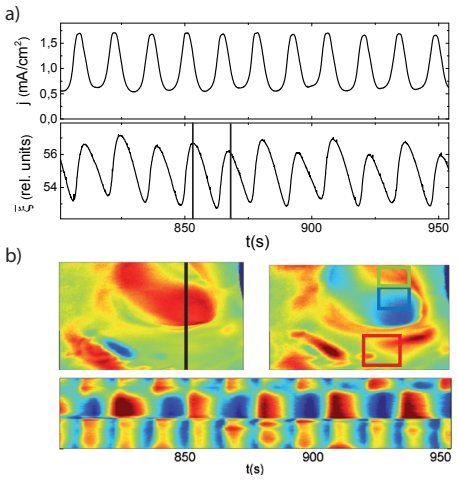

Figure 15: Analysis of a pattern consisting of a 2-phase cluster and a desynchronized region ($c_F = 100$ mM, pH = 3.5, $R_{ext}A = 2.81$ kΩcm^2, $I_{ill} = 2.7$ mW/cm^2). **a)** Time series of j and $\bar{\xi}$; **b)** Ellipsometric intensity distribution on the electrode for the two times indicated by the vertical lines in a) and the temporal evolution of a 1d cut along the line indicated in the left electrode picture. Red indicates a relatively high and blue a relatively low ellipsometric intensity.

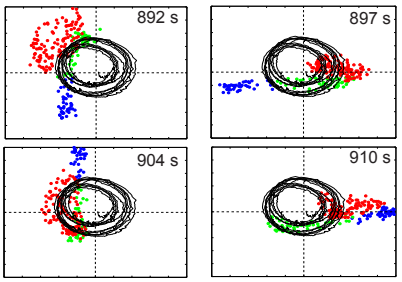

Figure 16: Analytical signal from the points indicated by correspondingly color coded rectangles in figure 15 b) at four points during two oscillation periods of the $\bar{\xi}$ oscillation shown in figure 15 a) together with the trace of the analytical signal of $\bar{\xi}$ (solid).

shown in figure 17. In the distribution of amplitude and phase of the Fourier coefficient of the subharmonic mode in the lower images of figure 17 c) the lack of balance between the phase domains of the 2-phase cluster becomes apparent. The difference between the unbalanced and the balanced case is visualized in figure 18 by an overlay of the amplitude and phase plots of the Fourier coefficients of the subharmonic mode for the patterns shown in figures 17 (unbalanced) and 10 (balanced), respectively. While the two phase domains on the left hand side of the unbalanced electrode in figure 18 are of similar size and the amplitude of the Fourier coefficient in these domains is similar, there is no counterbalancing phase domain for the domain in the upper right corner. For this reason the phase color coded as purple in figure 17 c) is also visible as an amplitude variation in the spatially averaged ellipsometric intensity signal. Whenever the average signal $\bar{\xi}$ of a patterned electrode oscillates with a period-2, unbalanced 2-phase clusters are present.

3.4 Irregular oscillations in $\bar{\xi}$

The last type of patterns discussed here occurs accompanied by an irregular oscillation of $\bar{\xi}$ as shown in the bottom of

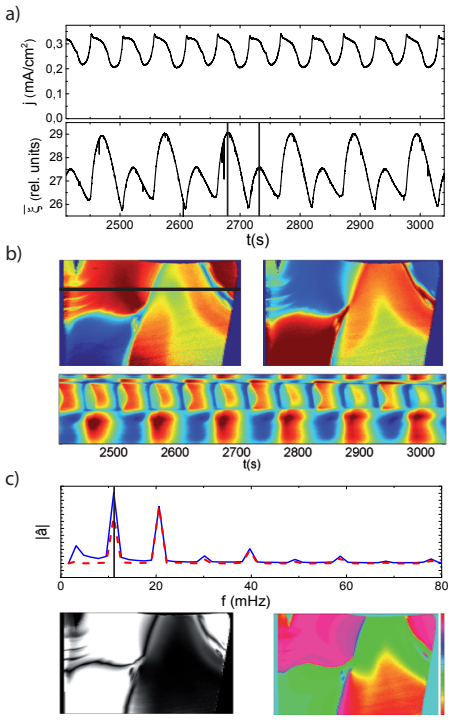

Figure 17: Analysis of a pattern consisting of a 2-phase cluster and a desynchronized region ($c_F = 50$ mM, pH = 1, $R_{ext}A = 2.61$ kΩcm^2, $I_{ill} = 0.4$ mW/cm^2). **a)** Time series of j and $\bar{\xi}$; **b)** Ellipsometric intensity distribution on the electrode for the two times indicated by the vertical lines in a) and the temporal evolution of a 1d cut along the line indicated in the left electrode picture. Red indicates a relatively high and blue a relatively low ellipsometric intensity; **c)** Fourier analysis of the pattern shown in a). Spatial average of the absolute values of the pointwise Fourier spectra (blue) and Fourier spectrum of the spatially averaged signal $\bar{\xi}$ (red) and the spatial distribution of the absolute value (left) and phase (right) of the Fourier coefficient corresponding to the Fourier mode indicated by the vertical line in the Fourier spectra.

figure 4. In this case three different pattern categories are distinguished. The first category, shown in figure 19, can again be seen as a deviation from the case of simple periodic spatial average oscillations. Here the irregular oscillation of the spatial average is imposed on the entire electrode and the relative intensity of the maxima and minima of $\bar{\xi}$ in figure 19 a) can be traced in the synchronized region in the lower part of the one dimensional cut in figure 19 b). A striking similarity between this type of pattern and the patterns forming accompanied by a simple periodic oscillation in $\bar{\xi}$ is that the regions on the electrode retain their respective dynamical behaviors and sizes until the measurement is finished. Spatially uniform oscillations with an irregular amplitude are also encountered with p-type [25, 26] and highly illuminated n-type silicon samples, i.e., in the absence of the nonlinear coupling. For this reason the measurement shown in figure 19 can be seen as a deviation from the 'chimera state' shown in figure 13. The former is caused by the nonlinear coupling imposed on a spatially uniform oscillation with irregular, most likely chaotic, dynamics, while the latter is caused by the nonlinear coupling acting on a simple periodic, spatially uniform oscillation.

The other two categories of patterns forming during os-

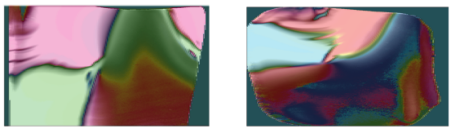

Figure 18: Comparison between the spatial distribution of absolute value and phase of the Fourier coefficients of a subharmonic cluster with different phase domain sizes and one with identical phase domain sizes.

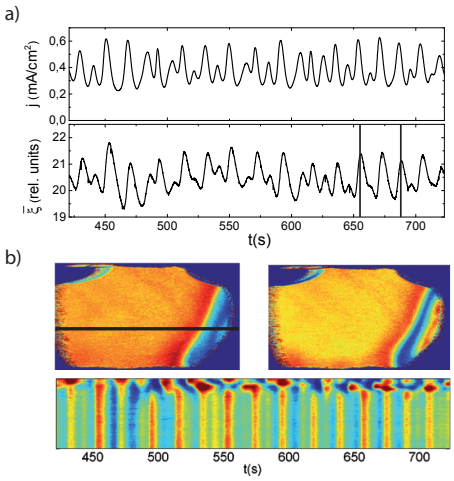

Figure 19: Analysis of a chimera type pattern occurring during an irregular $\bar{\xi}$ oscillation ($c_F = 75$ mM, pH = 1, $R_{ext}A = 6.51$ kΩcm^2, $I_{ill} = 3.0$ mW/cm^2). **a)** Time series of j and $\bar{\xi}$; **b)** Ellipsometric intensity distribution on the electrode for the two times indicated by the vertical lines in a) and the temporal evolution of a 1d cut along the line indicated in the left electrode picture. Red indicates a relatively high and blue a relatively low ellipsometric intensity.

cillations of $\bar{\xi}$ with an irregular amplitude are qualitatively different from all other types of patterns considered so far. The most important difference is that the regions spontaneously forming on the electrode, while still well distinguishable, show dynamical behavior varying with time. A first example of such spatio-temporal pattern formation is shown in figure 20. One important feature the spatio-temporal pattern shown in figure 20 shares with all spatio-temporal patterns shown so far, is that the regions with distinct dynamical behavior do not change their shape as is well visible in the temporal evolution of the cross section in figure 20 b). Conversely, the dynamical behavior in the region in the middle of the cross section changes significantly twice on a long time scale from a completely desynchronized oscillation pattern to a nearly synchronized oscillation pattern with a significantly lower amplitude and back. These profound changes in the overall behavior are also visible in the time series of $\bar{\xi}$.
Another qualitatively different behavior where the walls of the regions themselves are moving is shown in figure 21. In this example the respective sizes of the two regions distinguishable on the electrode surface change as one region first grows at the expense of the other to completely vanish once it fills up the entire electrode. It is remarkable in this example how long the memory of the surface seems to be as the period of the growing process is about 30 times larger than the base oscillation period.

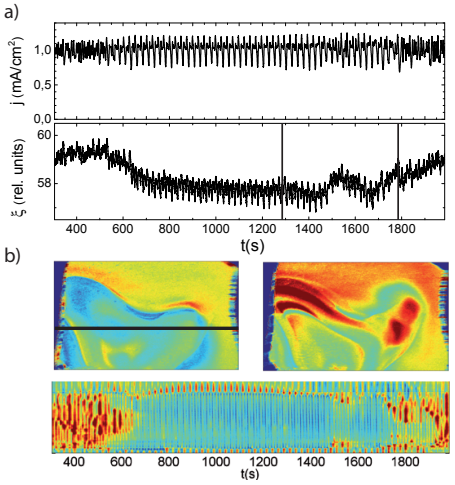

Figure 20: Analysis of a spatio-temporal pattern showing temporarily changing dynamical behavior within regions with stable walls ($c_F = 60$ mM, pH = 2.3, $R_{ext}A = 2.41$ kΩcm^2, $I_{ill} = 1.0$ mW/cm^2). **a)** Time series of j and $\bar{\xi}$; **b)** Ellipsometric intensity distribution on the electrode for the two times indicated by the vertical lines in a) and the temporal evolution of a 1d cut along the line indicated in the left electrode picture. Red indicates a relatively high and blue a relatively low ellipsometric intensity.

4 Summary and Conclusions

In this work we presented a variety of self-organized spatio-temporal patterns forming in the ellipsometric intensity during the oscillatory photoelectrodissolution of n-type silicon under limited illumination. Remarkably, complementary regions of distinct dynamical behavior formed spontaneously under completely uniform experimental parameters and without any external feedback. We classified these patterns by the behavior of the spatially averaged oscillation of the ellipsometric intensity $\bar{\xi}$, the dominant case being a simple periodic oscillation of $\bar{\xi}$. In this case, the patterns included synchronized oscillations, subharmonic 2-phase clusters emerging from the uniform oscillation by a period doubling bifurcation and desynchronized oscillations. Any pairwise coexistence of such dynamical regions was found including so-called 'chimera states'. The conservation of the simple periodic oscillation of $\bar{\xi}$ and j suggest the presence of a nonlinear global coupling. Indeed, the patterns only occur when the total coupling was found to be dominated by the nonlinear coupling imposed by the limited illumination. However, whether the coupling induced by the limited illumination of the sample is indeed global, remains an open question at this point. In addition to the case of simple periodic oscillations in $\bar{\xi}$, patterns accompanied by period-2 and irregular oscillations in $\bar{\xi}$ have been presented. In the former case the corresponding pattern forming could always be linked to the occurrence of an unbalanced subharmonic 2-phase cluster. The latter case opens a wide variety of possible patterns which were classified by the stability of the region walls and their long term behavior but not yet studied in detail.

The study reveals important open questions concerning the dynamics of silicon electrodissolution as well as universal laws governing pattern formation in oscillatory media. Among the former is the physical mechanism which leads to the conserved oscillation of the spatially averaged quantities. This should be closely related to the dynamics of holes under

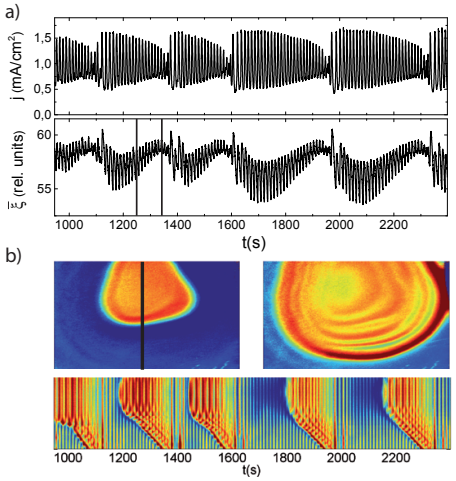

Figure 21: Analysis of a spatio-temporal pattern showing periodical changes in the region sizes (c_F = 100 mM, pH = 3.5, $R_{ext}A$ = 4.22 kΩcm^2, I_{ill} = 2.7 mW/cm^2). **a)** Time series of j and $\bar{\xi}$; **b)** Ellipsometric intensity distribution on the electrode for the two times indicated by the vertical lines in a) and the temporal evolution of a 1d cut along the line indicated in the left electrode picture. Red indicates a relatively high and blue a relatively low ellipsometric intensity.

illumination limited reaction conditions. As for the latter, the conserved oscillation of the spatially averaged quantities seems to strongly promote the spontaneous emergence of the coexistence of different dynamical states on the electrode. In a wider sense, this can be seen as diversification of the dynamical behavior of a system with uniform parameters. The role of self-organization for the emergence of differentiation in uniform systems is a central problem in non-linear dynamics, having implications in diverse fields such as biology or sociology, e.g., in decision making processes.

Acknowledgments

We thank our Bachelor students Martin Wiegand and Elmar Mitterreiter for carrying out some of the experiments shown and Iljana Miethe and Lennart Schmidt for fruitful discussions. Financial support from DFG (Grant KR1189/12-1) and the cluster of excellence 'Nanosystems Initiative Munich' (NIM) is gratefully acknowledged.

References

References

[1] Y. Kuramoto. *Chemical oscillations, waves, and turbulence*. Dover Publications, Inc. (Mineola, New York), 1984.

[2] M.C. Cross and P.C. Hohenberg. Pattern formation outside of equilibrium. *Rev. of Mod. Phys.*, 65(3):851, 1993.

[3] A.N. Zaikin and A.M. Zhabotinsky. Concentration wave propagation in two-dimensional liquid-phase self-oscillating system. *Nature*, 225:535, 1970.

[4] I.R. Epstein and K. Showalter. Nonlinear chemical dynamics: Oscillations, patterns, and chaos. *J. Phys. Chem.*, 100:13132, 1996.

[5] S. Jakubith, H. H. Rotermund, W. Engel, A. von Oertzen, and G. Ertl. Spatiotemporal concentration patterns in a surface reaction: Propagating and standing waves, rotating spirals, and turbulence. *Phys. Rev. Lett.*, 65(24):3013, 1990.

[6] G. Ertl. Oscillatory kinetics and spatio-temporal selforganization in reactions at solid surfaces. *Science*, 254:1750, 1991.

[7] M. Meixner, P. Rodin, E. Schöll, and A. Wacker. Lateral current density fronts in globally coupled bistable semiconductors with s- or z-shaped current voltage characteristics. *Eur. Phys. J. B*, 13:157, 2000.

[8] E. Schöll. *Nonlinear spatio-temporal dynamics and chaos in semiconductors*. Cambridge University Press, 2001.

[9] H.-G. Purwins, H. U. Bödeker, and S. Amiranashvili. Dissipative solitons. *Adv. in Phys.*, 59:485, 2010.

[10] N. Mazouz, G. Flätgen, and K. Krischer. Tuning the range of spatial coupling in electrochemical systems: From local via nonlocal to global coupling. *Phys. Rev. E*, 55(3):2260, 1997.

[11] J. Christoph and M. Eiswirth. Theory of electrochemical pattern formation. *Chaos*, 12:215, 2002.

[12] K. Krischer, H. Varela, A. Birzu, F. Plenge, and A. Bonnefont. Stability of uniform electrode states in the presence of ohmic drop compensation. *Electrochim. Acta*, 49:103, 2003.

[13] H. Varela, C. Beta, A. Bonnefont, and K. Krischer. Transitions to electrochemical turbulence. *Phys. Rev. Lett.*, 94:174104, 2005.

[14] M. Falcke, H. Engel, and M. Neufeld. Cluster formation, standing waves, and stripe patterns in oscillatory active media with local and global coupling. *Phys. Rev. E*, 52:763, 1995.

[15] V.K. Vanag, L. Yang, M. Dolnik, A.M. Zhabotinsky, and I.R. Epstein. Oscillatory cluster patterns in a homogeneous chemical system with global feedback. *Nature*, 406:389, 2000.

[16] W. Wang, I.Z. Kiss, and J.L. Hudson. Experiments on arrays of globally coupled chaotic electrochemical oscillators: Synchronization and clustering. *Chaos*, 10:248, 2000.

[17] M. Bertram, C. Beta, M. Pollmann, A.S. Mikhailov, H.H. Rotermund, and G. Ertl. Pattern formation on the edge of chaos: Experiments with CO oxidation on a Pt(110) surface under global delayed feedback. *Phys. Rev. E*, 67:036208, 2003.

[18] H. Varela, C. Beta, A. Bonnefont, and K. Krischer. A hierarchy of global coupling induced cluster patterns during the oscillatory H_2-electrooxidation reaction on a Pt ring-electrode. *Phys. Chem. Chem. Phys.*, 7:2429, 2005.

[19] V. Hakim and W.-J. Rappel. Dynamics of the globally coupled complex ginzburg-landau equation. *Phys. Rev. A*, 46:7347, 1992.

[20] K. Okuda. Variety and generality of clustering in globally coupled oscillators. *Physica D*, 63:424, 1993.

[21] X. G. Zhang. *Electrochemistry of silicon and its oxides*. Kluwer Academic, 2001.

[22] H. Hasegawa, S. Arimoto, J. Nanjo, H. Yamamoto, and H. Ohno. Anodic oxidation of hydrogenated amorphous silicon and properties of oxide. *J. Electrochem. Soc.*, 135(2):424, 1988.

[23] J.S. Judge. A Study of the Dissolution of SiO_2 in Acidic Fluoride Solutions. *J. Electrochem. Soc.*, 118(11):1772, 1971.

[24] S. Cattarin, I. Frateur, M. Musiani, and B. Triboullet. Electrodissolution of p-Si in acidic fluoride media. *J. Electrochem. Soc.*, 147:3277, 2000.

[25] I. Miethe and K. Krischer. Ellipsomicroscopic studies of the anodic oxidation of p-type silicon in fluoride containing electrolytes during current oscillations. *J. Electroanal. Chem.*, 666:1, 2012.

[26] K. Schönleber and K. Krischer. High-amplitude versus low-amplitude current oscillations during the anodic oxidation of p-type silicon in fluoride containing electrolytes. *Chem. Phys. Chem.*, 13:2989, 2012.

[27] K. Krischer, N. Mazouz, and G. Flätgen. Pattern formation in globally coupled electrochemical systems with s-shaped current-potential curve. *J. Phys. Chem. B*, 104:7545, 2000.

[28] K. Krischer. *Advances in Electrochemical Science and Engineering Vol. 8*, chapter 2, pages 90–203. Wiley-VCH Verlag GmbH & Co. KGaA, 2002.

[29] I. Miethe, V. Garcia-Morales, and K. Krischer. Irregular subharmonic cluster patterns in an autonomous photoelectrochemical oscillator. *PRL*, 102:194101, 2009.

[30] V. Garcia-Morales, A. Orlov, and K. Krischer. Subharmonic phase clusters in the complex ginzburg-landau equation with nonlinear global coupling. *Phys. Rev. E*, 82:065202, 2010.

[31] L. Schmidt, K. Schönleber, K. Krischer, and V. Garcia-Morales. Coexistence of synchrony and incoherence in oscillatory media under nonlinear global coupling. *Chaos*, 24(1):013102, 2014.

[32] Y. Kuramoto and D. Battogtokh. Coexistence of coherence and incoherence in nonlocally coupled phase oscillators. *Nonlin. Phenom. in Complex Syst.*, 5:380, 2002.

[33] D. M. Abrams and S. H. Strogatz. Chimera states for coupled oscillators. *Phys. Rev. Lett.*, 93:174102, 2004.

[34] A. M. Hagerstrom, T. E. Murphy, R. Roy, P. Hövel, I. Omelchenko, and E. Schöll. Experimental observation of chimeras in coupled-map lattices. *Nature Phys.*, 8:658, 2012.

[35] M. R. Tinsley, N. Simbarashe, and K. Showalter. Chimera and phase-cluster states in populations of coupled chemical oscillators. *Nature Phys.*, 8:662, 2012.

[36] E. A. Martens, S. Thutupalli, A. Fourrire, and O. Hallatschek. Chimera states in mechanical oscillator networks. *Proc. Natl. Acad. Sci.*, 110(26):10563, 2013.

[37] M. Wickramasinghe and I.Z. Kiss. Spatially organized dynamical states in chemical oscillator networks: Synchronization, dynamical differentiation, and chimera patterns. *PLoS One*, 8:e80586, 2013.

[38] A.G. Smart. Exotic chimera dynamics glimpsed in experiments. *Physics Today*, 65(10):17, 2012.